Vesicle capture by membrane-bound Munc13-1 requires selfassembly into discrete clusters

Feng Li, Venkat Kalyana Sundaram, Alberto T Gatta, Jeff Coleman, Sathish Ramakrishnan, Shyam S Krishnakumar, Frederic Pincet, James E Rothman

▶ **To cite this version:**

Feng Li, Venkat Kalyana Sundaram, Alberto T Gatta, Jeff Coleman, Sathish Ramakrishnan, et al.. Vesicle capture by membrane-bound Munc13-1 requires selfassembly into discrete clusters. FEBS Letters, 2021, 595 (17), pp.2185-2196. 10.1002/1873-3468.14157 . hal-03297036

HAL Id: hal-03297036

https://hal.sorbonne-universite.fr/hal-03297036

Submitted on 23 Jul 2021

HAL is a multi-disciplinary open access archive for the deposit and dissemination of scientific research documents, whether they are published or not. The documents may come from teaching and research institutions in France or abroad, or from public or private research centers.

L'archive ouverte pluridisciplinaire **HAL**, est destinée au dépôt et à la diffusion de documents scientifiques de niveau recherche, publiés ou non, émanant des établissements d'enseignement et de recherche français ou étrangers, des laboratoires publics ou privés.

Vesicle capture by membrane-bound Munc13-1 requires self-assembly into discrete clusters

Feng Li[1,2], Venkat Kalyana Sundaram[1,2], Alberto T. Gatta[1,2,3], Jeff Coleman[1,2], Sathish Ramakrishnan[1,2], Shyam S. Krishnakumar[1,2], Frederic Pincet[1,2,4,*], and James E. Rothman[1,2,*]

[1]Department of Cell Biology, School of Medicine, Yale University, 333 Cedar Street, New Haven, CT 06520, USA

[2]Nanobiology Institute, Yale School of Medicine, West Haven, CT 06516, USA

[3]Present address: The Francis Crick Institute, 1 Midland Road, London, NW1 1AT, United Kingdom

[4]Laboratoire de Physique de l'Ecole normale supérieure, ENS, Université PSL, CNRS, Sorbonne Université, Université de Paris, F-75005 Paris, France

* Correspondence to James E. Rothman or Frederic Pincet

Email: james.rothman@yale.edu, frederic.pincet@ens.fr

Keywords: Munc13-1, cluster, SNARE, synaptic vesicle, neurotransmission, membrane fusion.

Abstract

Munc13-1 is a large banana-shaped soluble protein that is involved in the regulation of synaptic vesicle docking and fusion. Recent studies suggest that multiple copies of Munc13-1 form nano-assemblies in active zones of neurons. However, it is not known if such clustering of Munc13-1 is correlated with multivalent binding to synaptic vesicles or specific plasma membrane domains at docking sites in the active zone. The functional significance of putative Munc13-1 clustering is also unknown. Here we report that nano-clustering is an inherent property of Munc13-1, and is indeed required for vesicle binding to bilayers containing Munc13-1. Purified Munc13-1 protein reconstituted onto supported lipid bilayers assembled into clusters containing from 2 to ~20 copies as revealed by a combination of quantitative TIRF microscopy and step-wise photobleaching. Surprisingly, only clusters containing a minimum of 6 copies of Munc13-1 were capable of efficiently capturing and retaining small unilamellar vesicles. The C-terminal C_2C domain of Munc13-1 is not required for Munc13-1 clustering, but is required for efficient vesicle capture. This capture is largely due to a combination of electrostatic and hydrophobic interactions between the C_2C domain and the vesicle membrane.

Introduction

Synaptic vesicle fusion is driven by the zippering of the membrane-proximal helices of v- and t-SNARE proteins Syntaxin1, SNAP25 and VAMP2 into a force-generating bundle termed a SNAREpin [1-3]. Syntaxin-1 is initially bound to a dedicated chaperone, Munc18-1, stabilizing a closed conformation that is unable to assemble with SNAP25 and VAMP2 to form a SNAREpin [4]. The central MUN domain of another protein, Munc13-1, binds Syntaxin-1 and weakens its interaction with Munc18 [5-8]. MUN also independently binds VAMP2 and co-operates with Munc18 to template SNAREpins [9].

Thus, the overall picture that emerges is that only when all three synaptic SNAREs are within molecular contact distance can they efficiently assemble into SNAREpins, a reaction catalyzed by their two co-operatively acting, specialized molecular chaperones, Munc18 and Munc13-1 [10]. This reaction, further coordinated by two proteins (Synaptotagmin-1 and Complexin) that co-operatively clamp the nascent SNAREpins to prevent membrane fusion until signaled by Ca^{2+}, primes the vesicles for release, creating what is referred to as the “readily-releasable pool”. Separately, but still just as important, Munc13-1 is necessary for local capture of the synaptic vesicles, as it is needed to bring them within molecular contact range to initiate the cascade of events just outlined [11,12].

Munc13-1 was identified from functional screens in nematodes and mammalian synapses [13,14], and independently as the phorbol ester receptor that mediates drug-enhanced neurotransmitter release [15,16]. Munc13-1 is a complex protein. Besides its molecule phorbol ester/diglyceride binding C_1 domain, it also contains three C_2 domains, and the MUN domain [17]. The MUN domain, which contains the chaperone activity of Munc13-1 is physically “banana”-shaped and about 15 nm long [18]. It is flanked by a C_1-C_2 (C_2B) unit at one end, and a distinct C_2 (C_2C) domain at the other end at the C-terminus of the protein. Its third C_2 unit (C_2A) resides at the N-terminus of the protein, and is important for the initial membrane capture of the synaptic vesicle at the active zone, much as the C-terminal C_2C domain is important for the closer, local capture of a vesicle to trigger SNAREpin assembly [11,12].

A recent super-resolution optical imaging study of neurons revealed that Munc13-1 exists in nano-assemblies of ~5-10 copies in the active zone of synapse, and that such clusters recruit Syntaxin-1 to the release sites of neurotransmitters [19]. The authors also show that the number of release sites are equal to the number of Munc13-1 clusters in the active zone [19,20]. This suggested that Munc13-1 clusters constitute the foundation and cornerstone of the release sites. This study also concluded that in order to get released, every synaptic vesicle has to bind to a Munc13-1 cluster; otherwise, the vesicle will reach a dead-end.

With this background in mind, we attempted to investigate further using a fully-defined system whether clustering is an inherent property of Munc13-1, and if these Munc13-1 clusters would be sufficient to capture vesicles. Here, we address these questions by testing the organization of Munc13-1 on supported lipid bilayers. We observed that Munc13-1 alone forms clusters and that at least 6 copies of the protein must be present to render the cluster potent for vesicle capture.

Results

Reconstituted Munc13-1 molecules form clusters on a lipid bilayer membrane

The mammalian (rat) Munc13-1 is a large molecule with 1735 amino acid residues. Here we used a truncated form of Munc13-1 in which the N-terminal C2A and Low Complexity Sequence domains are deleted. This deletion has been found to have minimal effects on synaptic transmission in hippocampal cultures, apart from a small decrease in the number of docked synaptic vesicles [12]. We attached a 12x His tag and a Halo tag to the N- and C-termini, respectively, of the $C_1C_2BMUNC_2C$ domains (residues 529 to 1735, Δ1408-1452, EF, Δ1533-1551) and expressed the construct in Expi293 mammalian cells [21]. High-quality protein was obtained through a Nickel-NTA affinity column purification procedure (Supplementary Figure S1). The C-terminal Halo tag allowed us to couple a single fluorophore, Alexa488, conjugated with Halo ligand (Supplementary Figure S1). Hereinafter, the resulting molecule is called $Munc13_L$.

We first made liposomes with DOPC, DOPS, PI(4,5)P2, and DAG (63:25:2:10, mol/mol, see Materials and Methods for acronyms and details) lipids by extrusion, and then bursted the liposomes at the bottom of an Ibidi flow cell [22] using $MgCl_2$. The resulting bilayer was uniform and smooth (Supplementary Figure S2). $Munc13_L$-Halo-Alexa488 (10 nM) in a buffer solution containing 50 mM HEPES, 140 mM KCl, 10% glycerol, and 1 mM DTT was then added on top of the bilayer. After incubation for 60 min, $Munc13_L$ molecules that were unbound to the bilayer were removed by extensive washing. The flow cell was then mounted on a TIRF microscope. We observed puncta formed by $Munc13_L$ on the bilayer membrane (Figure 1A). In contrast, when there was no lipid bilayer membrane, very few $Munc13_L$ particles were observed on the glass bottom of a bare flow cell (Figure 1B).

To determine the number of copies of $Munc13_L$ in each puncta, we gradually bleached the image frames using suitable laser power at different positions (Supplementary Movie 1). The bleaching profiles (particle fluorescence intensity versus time) were plotted and a variety of bleaching patterns were found. When the $Munc13_L$ copy number was small, the bleaching profile displayed apparent discrete steps, and the actual number of proteins can be determined from counting the number and intensity of steps. For example, 6 bleaching steps were found in Figure 1C, each

step corresponding to the bleaching of one or two Munc13$_L$ molecules. This method only works for relatively small copy numbers (generally 5 to 6 or fewer) because the bleaching profile becomes smooth when the copy number is large (Figure 1D). As an alternative for larger copy numbers, we fitted the intensity profile using

$$I(t) = I_0 e^{-t/\tau} + B$$

where $I(t)$ is the intensity at time t, I_0 is the initial intensity before bleaching, τ is the time constant, and B is the background (Supplementary Figure S3). Hence the copy number N can be obtained through

$$N = I_0/i$$

where i is the unit intensity of a single fluorophore or the average intensity of a single bleaching step determined using small clusters.

The histogram of the copy number shows that the size of the clusters has a broad distribution from 1 to 18 molecules (Figure 1E) with a large fraction of smaller oligomers. The existence of clusters with a large number of Munc13 shows that the size is not regulated. The average density of clusters is about 5 ± 1 clusters per 1000 μm^2. Therefore the average distance between the two nearest neighboring clusters is 14 $\pm$ 2 μm. This suggests that the Munc13-1 clusters are well separated from each other and must form independently.

In principle there are two possible ways Munc13$_L$ clusters could form: (i) the clusters could self-assemble via direct contacts between the Munc13$_L$ molecules themselves; or (ii) Munc13$_L$ molecules could independently bind to a common sub-resolution (<250 nm) lipid domain enriched for example in PIP2 and/or other lipids [23], and simply appear to be molecularly colocalized within such lipid domains.

We realize that it is difficult to determine the packing and interaction between Munc13-1 molecules in the cluster without sub-atomic structural data from x-ray crystallography or cryo electron microscopy. High-resolution structural studies will likely differentiate between these two origins of Munc13 clustering.

Munc13$_L$ clusters stably capture vesicles to lipid bilayer membranes

Next we tested the ability of $Munc13_L$ clusters to stably capture vesicles. We incubated the $Munc13_L$-bound bilayer with vesicles containing DOPC, DOPS, DOPE-Atto647N (68:30:2, mol/mol, see Materials and Methods for details), followed by an extensive buffer wash, so that only vesicles that were stably bound to the membrane would remain. Clusters of $Munc13_L$ and captured vesicles were independently imaged in the 488 nm and 633 nm channels, respectively (Figure 2A). The average density of vesicles on the lipid bilayer membrane was 2.5 ± 0.5 vesicles per 1000 μm^2.

Merging the images from these two channels revealed that $75 \pm 15\%$ of all the membrane-attached vesicles were colocalized with $Munc13_L$ clusters (Figure 2A). As a control, we incubated vesicles with the bilayer membrane in the absence of Munc13-1 (Figure 2B). The average density of vesicles on the lipid bilayer membrane dramatically decreased to ~ 0.5 vesicles per 1000 μm^2, which was similar to the density of vesicles not co-localized with $Munc13_L$ in Figure 2A, suggesting these non-colocalized vesicles were non-specifically attached to the bilayer.

Thus, $Munc13_L$ clusters are inherently able to capture vesicles from solution and stably tether them to the bilayer membrane. Previous studies related to Munc13-1 capture of vesicles have either been *in vivo*, showing Munc13-1 is necessary for vesicle recruitment but not clarifying whether Munc13-1 acts directly on the capture [12] or they have been in defined systems showing clustering of homogeneous vesicles [11,17], a process that is not necessarily related to vesicle capture of heterotypic vesicles by plasma membrane. When VAMP2 and Synaptotagmin-1 were reconstituted to vesicles, they did not influence Munc13-1's function of capturing vesicles (Supplementary Figure S4). We choose to use VAMP2-free and Synaptotagmin-1-free vesicles, because such system eliminates the possibilities that Synaptotagmin-1 interacts with PI(4,5)P2 on bilayers and Munc13-1 interacts with VAMP2, so that we can study Munc13-1's intrinsic properties.

$Munc13_L$ clusters must be at least hexameric to capture vesicles

Not all the $Munc13_L$ clusters captured vesicles in the previous experiments (Figure 2A). To establish whether there is relationship between the size of a $Munc13_L$ cluster and its capacity for vesicle capture, we determined the copy number of each cluster on the image frame from the step-bleaching profiles and recorded whether or not it had captured a vesicle (Figure 3A). We examined the data sets from 5 image frames drawn from independent experiments. Figure 3B reveals that the copy number distributions of $Munc13_L$ clusters that have captured a vesicle (red) and those that have not (blue) are markedly different. A distinct transition was observed: most

clusters that did not capture a vesicle had 5 or fewer copies of Munc13$_L$, whereas those clusters that had stably captured a vesicle contained 6 or more Munc13$_L$ copies.

Drawing on the same data set, we also calculated the probability that a cluster captured a vesicle as a function of the number of Munc13$_L$ molecules in the cluster (Figure 3C). This analysis revealed that clusters containing 6 or more copies of Munc13$_L$ had a nearly 100% probability of stably capturing a vesicle, and this probability becomes insignificant when there are fewer than 5 copies.

We conclude that a hexameric cluster contains the minimum threshold number of copies of Munc13$_L$ needed to reliably and stably capture a single vesicle in a fully-defined system.

The C_2C domain is required for vesicle capture but not for clustering

The C-terminal C_2 domain of Munc13-1, C_2C domain, was reported to be important in bridging liposome vesicle membranes [11]. To test whether this domain affects the formation of Munc13 clusters and their ability to capture vesicles, we generated a construct in which the C_2C domain was deleted. Like the Munc13$_L$ containing C_2C, a Halo tag was added on the C-terminus for subsequent labeling. This C_1C_2BMUN-Halo construct, amino acid residues 529 to 1531 (Δ1408-1452, EF), is well expressed in Expi293 cells. Protein was purified using a Nickel-NTA affinity column and further by size-exclusion chromatography. Purified protein was then labeled using the Halo ligand conjugated with Alexa488, so that a single fluorophore was coupled to every protein. We call this resulting protein Munc13$_S$ (Supplementary Figure S1).

As done previously, we then prepared bilayers containing PC, PS, PIP2, and DAG lipids. The bilayers were incubated with Munc13$_S$. After washing away the unbound protein, puncta formed by Munc13$_S$ were observed on the bilayer membrane (Figure 4A). These particles displayed comparable features as the clusters formed by Munc13$_L$ containing the C_2C domain.

When puncta of Munc13$_S$ on bilayers were gradually bleached using appropriate laser power, as noted before a mixture of large clusters with high initial intensity and continuous and smooth bleaching profiles, and small clusters with lower initial intensity could be observed (Supplementary Movie 2). Using the same analytical methods as before, we found that the size distribution of the Munc13$_S$ clusters was similar to the distributions of Munc13$_L$ clusters containing the C_2C domain, (Figure 4B). This result establishes that the C_2C domain is not involved in the self-assembly process that results in the observed clustering of Munc13-1.

We also studied another shorter mutant of Munc13-1, $Munc13_{1516}$ (residues 529 to 1516, Supplementary Figure S1), in which the hydrophobic linker between the MUN and the C_2C domain is removed from $Munc13_S$ [11]. As expected, this mutant is also able to form clusters with similar distribution on a lipid bilayer containing PC, PS, DAG, and PIP2 (Figure 4C and 4D).

To test for vesicle capture, the bilayer samples were incubated with vesicles containing DOPC, DOPS, and DOPE-Atto647N (68:30:2, mol/mol). Despite the similarity in size distribution between Munc13-1 clusters using $Munc13_L$ and the two C-terminal truncated mutants, the image frames in the 633 nm channel shows that the number of vesicles bound to the $Munc13_S$ bilayer was markedly decreased (Supplementary Figure S5) and further decreased when using $Munc13_{1516}$ (Supplementary Figure S6).

To quantify this reduced potency to capture vesicles, we correlated the size of $Munc13_S$ and $Munc13_{1516}$ clusters with the presence of colocalized vesicles. For $Munc13_S$ clusters, the likelihood of vesicles capture was reduced by more than half even when they contained 6 or more copies of $Munc13_S$ molecules (Figure 5A). This demonstrates that the C_2C domain of Munc13-1 plays a significant role in vesicle capture, possibility by directly interacting with the vesicle membrane. Binding efficiency of vesicles containing PC and PS to $Munc13_{1516}$ clusters is further decreased when compared with the efficiency to $Munc13_L$ clusters (Figures 5B and Supplementary Figure S6). Since the difference between these two mutants, $Munc13_S$ and $Munc13_{1516}$, is the removal of residues 1517 to 1531, a hydrophobic portion between MUN and C_2C domains, this suggests that the hydrophobic interaction between the vesicle and this short sequence may be the reason for the residual binding after deletion of the C_2C domain. Considering this portion is not exposed when the C_2C domain is not deleted [11] and hence has no contribution to vesicle binding in un-truncated Munc13-1, we assume that the C_2C domain is the main functional unit for vesicle binding.

We then removed the negatively charged lipids on the vesicle membrane by using only PC and PE-Atto647N (98:2, mol/mol). Binding efficiency of such neutral vesicles to clusters formed by the long version of $Munc13_L$ (residues 529 to 1735) is largely decreased to ~40% (Figure 5C and Supplementary Figures S7 and S8). This reduction is caused by the lack of electrostatic interaction between the negatively charged lipids on the vesicle and the positively charged residues on the C_2C domain. The remaining interactions, which are likely due to hydrophobic interaction between vesicle membrane and C_2C, may account for the remaining vesicle binding. This is consistent with the experiments conducted using cultured neurons, which suggest such hydrophobic interactions have a significant role, because the size of the readily releasable pool of

synaptic vesicles is largely reduced if one hydrophobic residue on C_2C is mutated to a charged residue (F1658E mutation) [11]

To summarize, our results show that cluster formation does not require the C_2C domain, but C_2C is crucial for Munc13-1's ability to capture vesicles. This capture is largely due to a combination of electrostatic and hydrophobic interactions between the C_2C domain and the vesicle membrane.

Discussion

In this study, we reconstituted Munc13-1 on lipid bilayer membranes and observed that the protein forms clusters containing 2 – 18 copies, determined from the step-bleaching of individual fluorescent dyes or from the initial fluorescent intensity of the cluster bleaching profiles. Clustering required binding to the bilayer and is an intrinsic property of the pure protein. Because we did not use super-resolution imaging, we cannot formally prove that the clusters exist through direct contacts among Munc13-1 molecules on the nano-scale, as distinct from consisting of individual, unassociated Munc13-1 molecules that we cannot optically resolve from each other. However, the fact that a unit of at least 6 such copies, clustered before vesicle binding within a single diffraction-limited region of bilayer surface, can cooperate to bind a common vesicle, places these 6 copies no further apart than the diameter of a ~50-100 nm small unilamellar vesicle. Several molecular arrangements can be envisioned for this Munc13-1 self-assembly into oligomers, either laterally side-to-side or end-to-end, or a combination. We cannot favor one or the other. However, the C_2C domain and hydrophobic linker are probably not involved because they are not required for cluster formation (Figure 4).

The surprising requirement that Munc13-1 clusters have to reach a critical copy number for vesicle capture is currently unexplained. Clusters with 4 or fewer Munc13-1 proteins can barely capture vesicles, whereas clusters of 6 or more capture vesicles with nearly perfect reliability. One possible explanation is that a single C_2C domain lacks sufficient affinity to reliably capture and stably retain a vesicle, and multivalent binding is required. This seems unlikely because multivalent interactions generally increase smoothly (and geometrically) with the degree of valency. The alternative is that the clusters present a specific architecture needed for binding that cannot form with less than a quorum of 6 subunits. This could be a hexameric arrangement of subunits in the known perpendicular (erect) topology, or it could be a co-planar hexameric ring of Mun13 on the surface of the bilayer [10], perhaps following a transition from initial capture in the perpendicular state.

What is the physiological consequence of our results? At presynaptic terminals, vesicles are drawn from reserve and recycling pools for capture at active zones to form the readily releasable pool that is primed for synchronous release. The SNAREs and Synaptotagmin-1 are known to bridge vesicles to the plasma membrane through membrane-insertion (SNAREpins) or binding (Synaptotagmin-1) to PIP2 based on supporting *in vivo* evidence [23-29]. Munc13-1 similarly is a strong candidate for a vesicle tether based on *in vitro* [11,17,30] and *in vivo* studies [11,12,31,32]. Our finding that hexameric clusters of Munc13-1 are minimally needed to reliably capture vesicles is consistent with the observation that ~5-10 copies are anatomically associated with each synaptic vesicle in the readily-releasable pool [19,20]. Our finding that the C_2C domain is the main functional unit for vesicle capture is also consistent with *in vivo* data and electron tomography results using hippocampal neurons [11], and the study of neurotransmitter release in *Caenorhabditis elegans* which suggests that the C2 domain at the C terminus of UNC-13 helps to bind synaptic vesicles to the plasma membrane [33]. Our data also suggest that both hydrophobic interaction and electrostatic interactions are important in vesicle binding to Munc13-1 clusters. These data are consistent with the *in vivo* study by Quade *et al* [11], which shows that the size of the readily releasable pool of cultured mouse neurons is significantly reduced by either removing the hydrophobic residue (F1658E mutation) or by reversing the charge from positive to negative (R1598E mutation) on the C_2C domain of Munc13-1. These similarities between our results and *in vivo* observations suggest that the clusters we describe here are of the same nature as the ones formed physiologically. Therefore, our work supports the prevailing model which states, *in vivo*, the Munc13-1 C_1C_2B domain binds to the plasma membrane, with the MUN domain rising up essentially perpendicular to the plasma membrane elevating and presenting the C_2C domain to capture synaptic vesicles [11,30].

This model is attractive because it elegantly explains the sequential hierarchy of physical limitations on vesicle-membrane separation at which initial capture can take place due to the different sizes of Synaptotagmin-1, SNAREs and Munc13-1. The interaction range of Munc13-1 is about 20 nm [18], whereas Synaptotagmin-1 can first interact with acidic lipids on plasma membrane at about 5 nm [34,35]. Zippering of the SNAREs is triggered when intermembrane distance is about 8 nm [25,36]. Assuming the capture of vesicles that we observed *in vitro* is mediated by a perpendicular arrangement of Munc13-1 in the clusters, this interaction will necessarily precede vesicle attachment by either Synaptotagmin-1 or SNAREs. If this is correct, nascent SNAREpins will have the opportunity to bind Synaptotagmins and Complexin [37] even before Synaptotagmin-1 can bind the plasma membrane and oligomerize. Also, it is entirely reasonable to imagine that the interactions with other synaptic proteins such as Syntaxin-1 and Synaptotagmin-1 could affect the degree of Munc13-1 oligomerization, thereby limiting its extent, and perhaps even shape uniform clusters that would facilitate vesicle capture and priming.

Materials and Methods

***Chemicals*.** The lipids used in this study, 1,2-dioleoyl-sn-glycero-3-phosphocholine (DOPC), 1-palmitoyl-2-oleoyl-sn-glycero-3-phosphocholine (POPC), 1,2-dioleoyl-sn-glycero-3-(phospho-L-serine) (sodium salt) (DOPS), L-α-phosphatidylinositol-4,5-bisphosphate (Brain, Porcine) (ammonium salt) (brain PI(4,5)P2), 1-2-dioleoyl-sn-glycerol (DAG), and 1,2-dioleoyl-sn-glycero-3-phosphoethanolamine-N-(7-nitro-2-1,3-benzoxadiazol-4-yl) (ammonium salt) (DOPE-NBD) were purchased from Avanti Polar Lipids. 1,2-Dioleoyl-sn-gylcero-3-phosphoethanolamine ATTO 647N (DOPE-Atto647N) was from ATTO-Tec. 4-(2-Hydroxyethyl)piperazine-1-ethanesulfonic acid (HEPES), Potassium hydroxide (KOH), Potassium chloride (KCl), Magnesium chloride ($MgCl_2$), Glycerol, DNAse I, RNAse A, Benzonase, Roche complete protease inhibitor cocktail tablets, Phorbol 12-myristate 13-acetate (PMA), and DL-Dithiothreitol (DTT) were purchased from Sigma-Aldrich. Nickel-NTA agarose, TCEP-HCl, and Expi293™ Expression System Kit were supplied by Thermo Fisher Scientific. The plasmid maxi prep kit was from QIAGEN. HaloTag® Alexa Fluor® 488 Ligand was purchased from Promega. All aqueous solutions were prepared using 18.2 MΩ ultra-pure water (purified with the Millipore MilliQ system).

Protein constructs, expression and purification.

The original vector expressing rat Munc13 was a kind gift from Dr. Claudio Giraudo. The plasmid expressing the Halo tag (pFN21A) was purchased from Promega. The expression plasmids His_{12}_PreScission _C_1_C_2B_MUN_C_2C_tev_Halo and His_{12}_PreScission _C_1_C_2B_MUN_tev_Halo (ΔC_2C Munc13) were produced by cloning rat Munc13-1 residues 529 to 1735 and 529 to 1531, respectively, to a mammalian cell expression vector between the BamHI and NotI sites. Munc13-1 residues 1408-1452 were deleted and residues EF were added in [5]. A short linker sequence containing a TEV cut site was subcloned in followed by the Halo tag. The resulting plasmids were amplified with maxi prep using QIAGEN Plasmid Maxi kit and were used to transfect Expi293F™ human cells. Proteins were expressed with Expi293™ expression system following the manufacturer's protocol. The three Munc13-1 proteins were then purified using Ni-NTA affinity beads as described before [38-40]. To summarize, the cell pellet was thawed on ice and disrupted with a homogenizer, and then spun in an ultracentrifuge for 30 minutes at ~142,400xg at 4°C. The supernatant was removed and 2 mL Qiagen Ni-NTA slurry along with 10 uL Benzonase were added, and subsequently rotated using an orbiting wheel overnight at 4°C. The beads were washed at 4°C with 30mL buffer containing 50 mM HEPES at pH 7.4, 400 mM KCl, 10% glycerol, 1 mM TCEP, and 10 mM Imidazole, then with another 30mL

buffer containing 50 mM HEPES at pH 7.4, 400 mM KCl, 10% glycerol, 1 mM TCEP, and 25 mM Imidazole, followed the third 30 mL buffer containing 50 mM HEPES at pH 7.4, 270 mM KCl, 10% glycerol, 1 mM TCEP, and 25 mM Imidazole. 100 μL of PreScission protease (~2 $mg.mL^{-1}$) in 1 mL buffer was added to the beads and incubated for 3 hours at room temperature with shaking to remove the 12xHis tag. After the cleavage reaction, elusions were collected and gel filtrated using a Superdex 200 column. The protein concentration was typically 1 to 2 $mg.mL^{-1}$ as determined by using a Bradford protein assay with Bovine Serum Albumin (BSA) as the standard.

Protein labeling

The three Munc13-1-Halo proteins were labeled by incubating the proteins with Alexa488 conjugated with HaloTag® from Promega, as described before [2]. The protein was first centrifuged at 14,000 rpm for 20 minutes at 4°C to remove any precipitation. Fluorescence dye was added into the protein solution at dye:protein = 5:1 molar ratio and the mixture was incubated for 30 min at room temperature with gentle rotation. Unreacted dye was removed by passing through the PD MidiTrap G-25 column (GE Healthcare) three times at room temperature. The labeling efficiencies were about 97%.

Liposome extrusion

Protein-free liposomes were prepared by extrusion using an Avestin mini-extruder [1]. The liposomes used to form bilayer membrane contained 63 mol% DOPC, 25 mol% DOPS, 2 mol% PI(4,5)P2, and 10 mol% DAG. The liposomes used for vesicle capture contained 68 mol% DOPC, 30 mol% DOPS, 2 mol% DOPE-Atto647N. Detailed description was included in the Supplementary Information.

Chloroform solutions of the lipid mixtures were dried with a nitrogen stream for 10 min, followed by vacuum drying for 1 hour. The thin lipid films were hydrated with 500 μL buffer containing 50 mM HEPES (pH 7.4), 140 mM KCl, and 10% glycerol. The mixture was vortexed vigorously for 30 minutes at room temperature. The multilamellar liposomes were frozen in liquid nitrogen for 30 sec, and were then thawed in a water bath at 37°C for 30 sec. This cycle was repeated eight times. Small unilamellar liposomes of ~100 nm were produced by extrusion through 100 nm polycarbonate filters using a Liposofast mini-extruder (Avestin) 21 times at room temperature.

Bilayer Preparation and TIRF microscopy

Bilayers were prepared by bursting liposomes on the glass surface of glass using a glass-bottomed μ-Slide $V1^{0.5}$ chip from Ibidi. 2.5 μL $MgCl_2$ at 500 mM were added into 122.5 μL buffer

containing 50 mM HEPES (pH 7.4), 140 mM KCl, and 10% glycerol. Then 125 µL extruded bilayer liposomes were added. 60 µL $MgCl_2$-liposome solution were loaded into the channel of the ibidi chip and incubate for 40 min at room temperature. The channel was washed with the same buffer supplemented with 6 mM EDTA, and then with buffer supplemented with 1 mM DTT. Depending on the purpose of experiments, $MgCl_2$ or $CaCl_2$ may be added in the buffer to the desired concentration. 60 µL of 10 nM Munc13-1-Halo-Alexa488 were loaded into the channel and incubate with the bilayer for 60 min at room temperature. The channel was washed with the buffer supplemented with 1 mM DTT. The vesicle liposomes were diluted 30 times. 60 µL diluted vesicle liposomes were loaded into the channel and incubate for 5 min at room temperature. The channel was washed with buffer supplemented with 1 mM DTT.

The Ibidi chip was then mounted to the stage of a Nikon TIRF microscope. Bilayers, Munc13 particles on bilayers, and vesicles attached to bilayers were respectively imaged at room temperature with the TIRF microscope using the corresponding laser.

Supplementary information

Supplementary Information includes: Supplementary Figures, and Supplementary Movies.

Author contributions

Feng Li, Conceptualization, Reagents, Data curation, Formal analysis, Investigation, Writing—original draft, Writing—review and editing; Venkat Kalyana Sundaram, Alberto T. Gatta, and Jeff Coleman, Reagents, Investigation, Writing—review and editing; Shyam S Krishnakumar, Frederic Pincet, and James E Rothman, Conceptualization, Formal analysis, Supervision, Funding acquisition, Writing—review and editing.

Acknowledgments

This work was supported by National Institute of Health (NIH) grant DK027044 to JER.

Data availability statement

The data that supports the findings of this study are available in Figures 1-5 and the supplementary material of this article .

References

[1] Li, F., Kummel, D., Coleman, J., Reinisch, K.M., Rothman, J.E. and Pincet, F. (2014). A Half-Zippered SNARE Complex Represents a Functional Intermediate in Membrane Fusion. J Am Chem Soc 136, 3456-64.

[2] Li, F., Tiwari, N., Rothman, J.E. and Pincet, F. (2016). Kinetic barriers to SNAREpin assembly in the regulation of membrane docking/priming and fusion. Proc Natl Acad Sci U S A 113, 10536-41.

[3] Francois-Martin, C., Rothman, J.E. and Pincet, F. (2017). Low energy cost for optimal speed and control of membrane fusion. Proc Natl Acad Sci U S A 114, 1238-1241.

[4] Baker, R.W., Jeffrey, P.D., Zick, M., Phillips, B.P., Wickner, W.T. and Hughson, F.M. (2015). A direct role for the Sec1/Munc18-family protein Vps33 as a template for SNARE assembly. Science 349, 1111-4.

[5] Yang, X. et al. (2015). Syntaxin opening by the MUN domain underlies the function of Munc13 in synaptic-vesicle priming. Nat Struct Mol Biol 22, 547-54.

[6] Ma, C., Li, W., Xu, Y. and Rizo, J. (2011). Munc13 mediates the transition from the closed syntaxin-Munc18 complex to the SNARE complex. Nat Struct Mol Biol 18, 542-9.

[7] Wang, S. et al. (2017). Conformational change of syntaxin linker region induced by Munc13s initiates SNARE complex formation in synaptic exocytosis. EMBO J 36, 816-829.

[8] Shu, T., Jin, H., Rothman, J.E. and Zhang, Y. (2020). Munc13-1 MUN domain and Munc18-1 cooperatively chaperone SNARE assembly through a tetrameric complex. Proc Natl Acad Sci U S A 117, 1036-1041.

[9] Wang, S., Li, Y., Gong, J., Ye, S., Yang, X., Zhang, R. and Ma, C. (2019). Munc18 and Munc13 serve as a functional template to orchestrate neuronal SNARE complex assembly. Nat Commun 10, 69.

[10] Rothman, J.E., Krishnakumar, S.S., Grushin, K. and Pincet, F. (2017). Hypothesis - buttressed rings assemble, clamp, and release SNAREpins for synaptic transmission. FEBS Lett 591, 3459-3480.

[11] Quade, B. et al. (2019). Membrane bridging by Munc13-1 is crucial for neurotransmitter release. Elife 8

[12] Camacho, M. et al. (2017). Heterodimerization of Munc13 C2A domain with RIM regulates synaptic vesicle docking and priming. Nat Commun 8, 15293.

[13] Brenner, S. (1974). The genetics of Caenorhabditis elegans. Genetics 77, 71-94.

[14] Brose, N., Hofmann, K., Hata, Y. and Sudhof, T.C. (1995). Mammalian homologues of Caenorhabditis elegans unc-13 gene define novel family of C2-domain proteins. J Biol Chem 270, 25273-80.

[15] Betz, A., Ashery, U., Rickmann, M., Augustin, I., Neher, E., Sudhof, T.C., Rettig, J. and Brose, N. (1998). Munc13-1 is a presynaptic phorbol ester receptor that enhances neurotransmitter release. Neuron 21, 123-36.

[16] Augustin, I., Rosenmund, C., Sudhof, T.C. and Brose, N. (1999). Munc13-1 is essential for fusion competence of glutamatergic synaptic vesicles. Nature 400, 457-61.

[17] Liu, X. et al. (2016). Functional synergy between the Munc13 C-terminal C1 and C2 domains. Elife 5

[18] Xu, J. et al. (2017). Mechanistic insights into neurotransmitter release and presynaptic plasticity from the crystal structure of Munc13-1 C1C2BMUN. Elife 6

[19] Sakamoto, H. et al. (2018). Synaptic weight set by Munc13-1 supramolecular assemblies. Nat Neurosci 21, 41-49.
[20] Ryan, T.A. (2018). Munc13 marks the spot. Nat Neurosci 21, 5-6.
[21] Fang, X.T., Sehlin, D., Lannfelt, L., Syvanen, S. and Hultqvist, G. (2017). Efficient and inexpensive transient expression of multispecific multivalent antibodies in Expi293 cells. Biol Proced Online 19, 11.
[22] Keeley, T.P., Siow, R.C.M., Jacob, R. and Mann, G.E. (2017). A PP2A-mediated feedback mechanism controls Ca(2+)-dependent NO synthesis under physiological oxygen. FASEB J 31, 5172-5183.
[23] Honigmann, A. et al. (2013). Phosphatidylinositol 4,5-bisphosphate clusters act as molecular beacons for vesicle recruitment. Nat Struct Mol Biol 20, 679-86.
[24] Park, Y. et al. (2015). Synaptotagmin-1 binds to PIP(2)-containing membrane but not to SNAREs at physiological ionic strength. Nat Struct Mol Biol 22, 815-23.
[25] Li, F., Pincet, F., Perez, E., Eng, W.S., Melia, T.J., Rothman, J.E. and Tareste, D. (2007). Energetics and dynamics of SNAREpin folding across lipid bilayers. Nat Struct Mol Biol 14, 890-6.
[26] Wang, Y.J., Li, F., Rodriguez, N., Lafosse, X., Gourier, C., Perez, E. and Pincet, F. (2016). Snapshot of sequential SNARE assembling states between membranes shows that N-terminal transient assembly initializes fusion. Proc Natl Acad Sci U S A 113, 3533-8.
[27] Stein, A., Radhakrishnan, A., Riedel, D., Fasshauer, D. and Jahn, R. (2007). Synaptotagmin activates membrane fusion through a Ca2+-dependent trans interaction with phospholipids. Nat Struct Mol Biol 14, 904-11.
[28] Arac, D. et al. (2006). Close membrane-membrane proximity induced by Ca(2+)-dependent multivalent binding of synaptotagmin-1 to phospholipids. Nat Struct Mol Biol 13, 209-17.
[29] Li, L., Shin, O.H., Rhee, J.S., Arac, D., Rah, J.C., Rizo, J., Sudhof, T. and Rosenmund, C. (2006). Phosphatidylinositol phosphates as co-activators of Ca2+ binding to C2 domains of synaptotagmin 1. J Biol Chem 281, 15845-52.
[30] Gipson, P., Fukuda, Y., Danev, R., Lai, Y., Chen, D.H., Baumeister, W. and Brunger, A.T. (2017). Morphologies of synaptic protein membrane fusion interfaces. Proc Natl Acad Sci U S A 114, 9110-9115.
[31] Brose, N., Rosenmund, C. and Rettig, J. (2000). Regulation of transmitter release by Unc-13 and its homologues. Curr Opin Neurobiol 10, 303-11.
[32] Betz, A. et al. (2001). Functional interaction of the active zone proteins Munc13-1 and RIM1 in synaptic vesicle priming. Neuron 30, 183-96.
[33] Padmanarayana, M. et al. (2021). A unique C2 domain at the C terminus of Munc13 promotes synaptic vesicle priming. Proc Natl Acad Sci U S A 118
[34] Wang, J. et al. (2014). Calcium sensitive ring-like oligomers formed by synaptotagmin. Proc Natl Acad Sci USA 111, 13966-71.
[35] Gruget, C., Coleman, J., Bello, O., Krishnakumar, S.S., Perez, E., Rothman, J.E., Pincet, F. and Donaldson, S.H., Jr. (2018). Rearrangements under confinement lead to increased binding energy of Synaptotagmin-1 with anionic membranes in Mg(2+) and Ca(2). FEBS Lett 592, 1497-1506.
[36] Li, F., Pincet, F., Perez, E., Giraudo, C.G., Tareste, D. and Rothman, J.E. (2011). Complexin activates and clamps SNAREpins by a common mechanism involving an intermediate energetic state. Nat Struct Mol Biol 18, 941-6.

[37] Zhou, Q., Zhou, P., Wang, A.L., Wu, D., Zhao, M., Sudhof, T.C. and Brunger, A.T. (2017). The primed SNARE-complexin-synaptotagmin complex for neuronal exocytosis. Nature 548, 420-425.
[38] Parlati, F., Weber, T., McNew, J.A., Westermann, B., Sollner, T.H. and Rothman, J.E. (1999). Rapid and efficient fusion of phospholipid vesicles by the alpha-helical core of a SNARE complex in the absence of an N-terminal regulatory domain. Proc Natl Acad Sci U S A 96, 12565-70.
[39] Ji, H., Coleman, J., Yang, R., Melia, T.J., Rothman, J.E. and Tareste, D. (2010). Protein determinants of SNARE-mediated lipid mixing. Biophys J 99, 553-60.
[40] Melia, T.J. et al. (2002). Regulation of membrane fusion by the membrane-proximal coil of the t-SNARE during zippering of SNAREpins. J Cell Biol 158, 929-40.

Figures and Tables

Figure 1. Munc13$_L$ forms clusters on a lipid bilayer. (**A**) & (**B**) Representative TIRF image of particles formed by Munc13$_L$ labeled with Alexa488 on a lipid bilayer membrane (**A**) and bare glass surface (**B**). (**C**) & (**D**) Representative step-bleaching profiles of Munc13$_L$ clusters of different sizes: small cluster (**C**), where the bleaching steps and corresponding numbers of dyes are indicated; and large cluster (**D**), where the bleaching profile displays a smooth decay. (**E**) Distribution of copy numbers in Munc13$_L$ clusters. Error bars represent *s.d., n=5*.

Figure 2. Munc13$_L$ clusters capture vesicles to lipid bilayer. (**A**) Munc13$_L$ clusters co-localize with vesicles that are captured onto a lipid bilayer from solution: TIRF image of clusters formed by Munc13$_L$ labeled with Alexa488 on a lipid bilayer (*left panel*), and TIRF image of vesicles containing PC, PS, and PE-Atto647N lipid that are anchored to a lipid bilayer (*middle panel*), and the merge of the previous two images (*right panel*). About ~75% of the vesicles on the lipid membrane are bound to Munc13$_L$ particles. (**B**) In the absence of Munc13-1, there is no specific capture of vesicles to the lipid bilayer: TIRF image of the Alexa488 channel (*left panel*), and TIRF image of vesicle containing DOPE-Atto647N lipid that are anchored to the lipid bilayer (*middle panel*), and the merge of the previous two images (*right panel*).

Figure 3. The copy number in Munc13$_L$ clusters needs to exceed a threshold value to be capable of capturing vesicles. (**A**) Mapping of copy numbers of Munc13$_L$ clusters in a representative image frame and capability of these clusters to capture vesicles that contain PC, PS, and PE-Atto67N. The numbers designate copy number of the clusters, and the red color

refers to clusters that are capable of capturing vesicles, whereas the blue color refers to clusters that incapable of capturing. (**B**) Correlation between copy numbers of $Munc13_L$ clusters and their capability of capturing vesicles. Copy number distribution of $Munc13_L$ clusters that are capable (red) and incapable (blue) of capturing vesicle, respectively. (**C**) Probability of capturing one or more vesicles by $Munc13_L$ clusters with different copy numbers.

Figure 4. C_2C domain and the hydrophobic linker do not affect Munc13-1 clustering. (**A**) & (**C**) Representative TIRF image of particles formed by $Munc13_S$ (residues 529 to 1531) (**A**) and $Munc13_{1516}$ (residues 529 to 1516) (**C**) labeled with Alexa488 on a lipid bilayer membrane, respectively. (B) & (D) Distribution of copy numbers in clusters particles formed by $Munc13_S$ (residues 529 to 1531) (B) and $Munc13_{1516}$ (residues 529 to 1516) (D). The dashed line is the size distribution of $Munc13_L$ clusters with C_2C domain, which serves as a reference.

Figure 5. C_2C domain is required for vesicle capture. (**A**) &(**B**) Probability of capturing vesicles that contain PC and PS by Munc13-1 clusters with different copy numbers. The clusters were formed by $Munc13_S$ (residues 529 to 1531) (**A**) and $Munc13_{1516}$ (residues 529 to 1516) (**B**). The dashed line is the same probability by $Munc13_L$ (residues 529 to 1735) clusters, which serves as a reference. (**C**) Probability of capturing vesicles that contain only PC, by $Munc13_L$ clusters. The dashed line is the probability of capturing vesicles that contain PC and PS by $Munc13_L$ clusters, which serves as a reference. This suggests $Munc13_L$ clusters still capture PC-only vesicles, but with reduced efficiency.

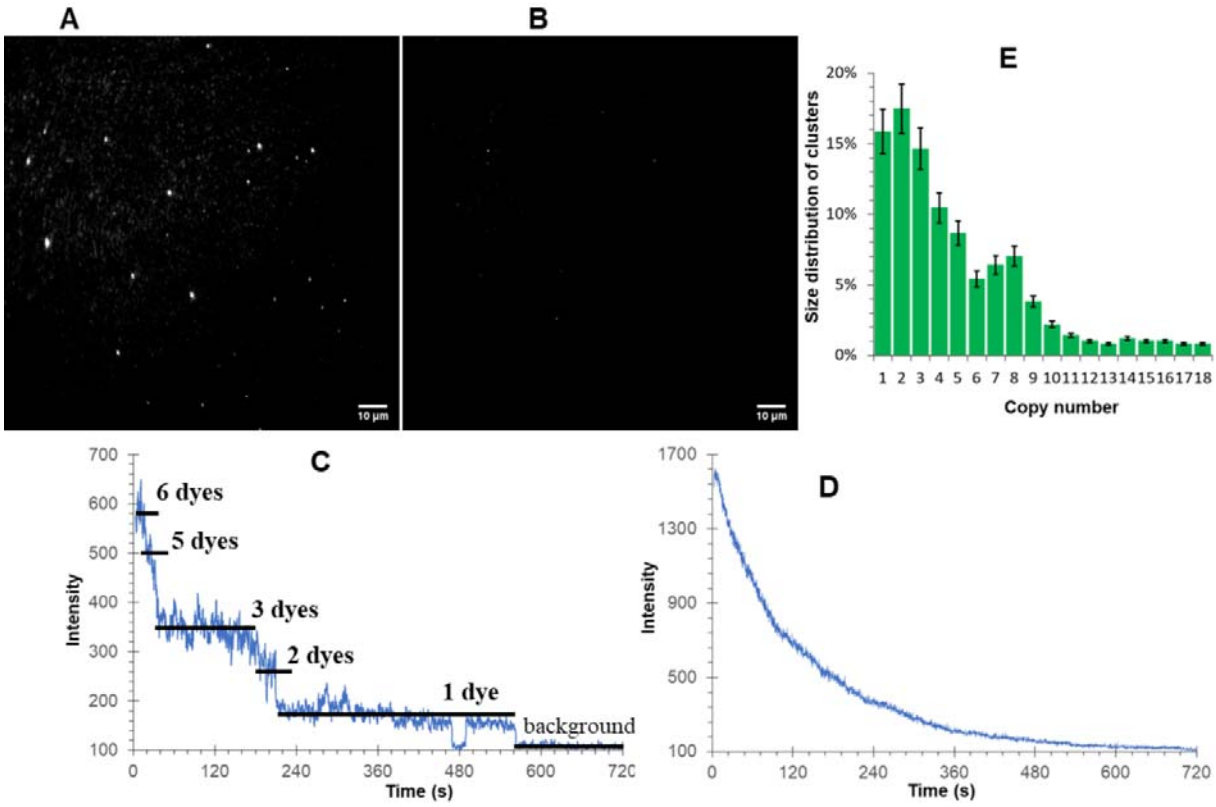
A
B
10 μm
10 μm
E
Size distribution of clusters
20%
15%
10%
5%
0%
1 2 3 4 5 6 7 8 9 10 11 12 13 14 15 16 17 18
Copy number
C
6 dyes
5 dyes
3 dyes
2 dyes
1 dye
background
Intensity
700
600
500
400
300
200
100
0 120 240 360 480 600 720
Time (s)
D
Intensity
1700
1300
900
500
100
0 120 240 360 480 600 720
Time (s)

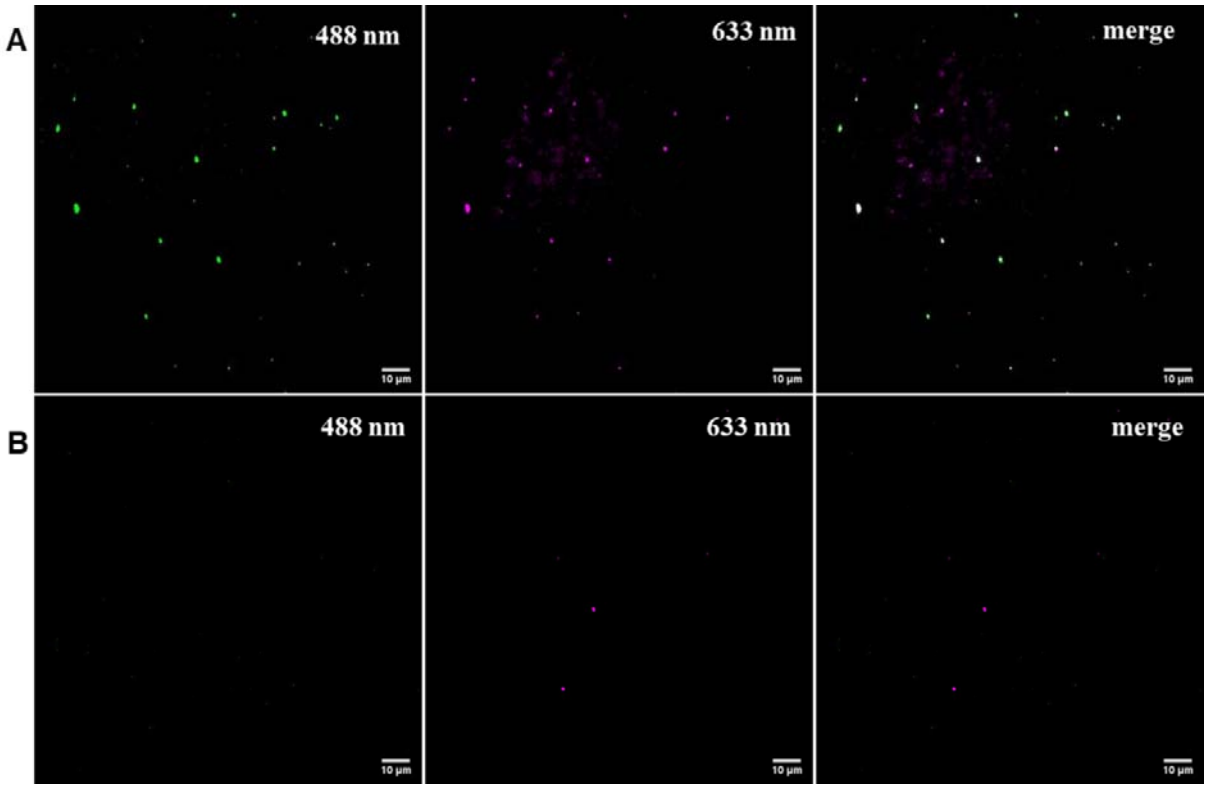
A
488 nm
633 nm
merge
B
488 nm
633 nm
merge

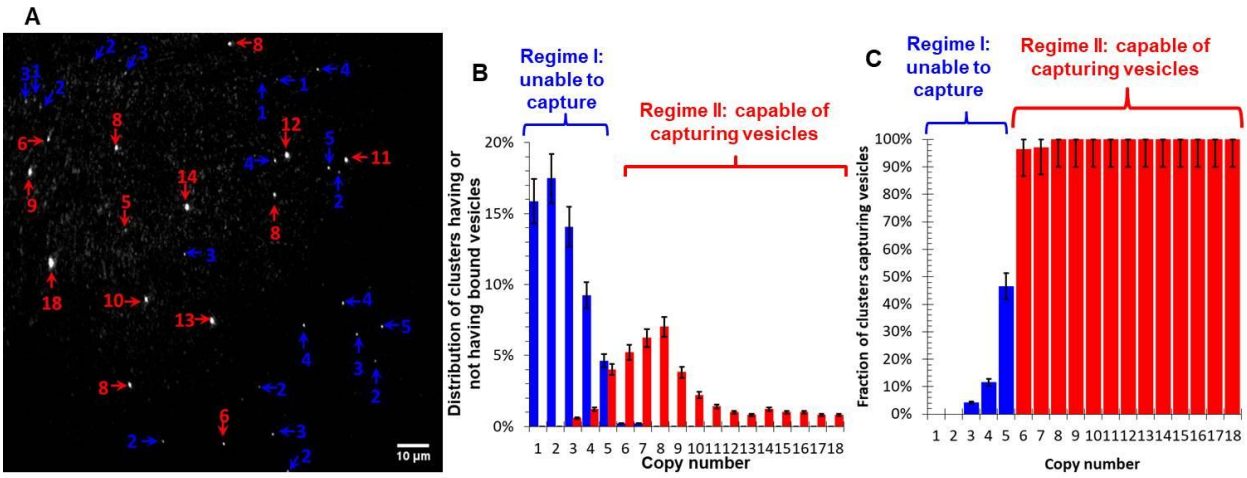
A
10 µm
B
Regime I: unable to capture
Regime II: capable of capturing vesicles
Distribution of clusters having or not having bound vesicles
Copy number
C
Regime I: unable to capture
Regime II: capable of capturing vesicles
Fraction of clusters capturing vesicles
Copy number

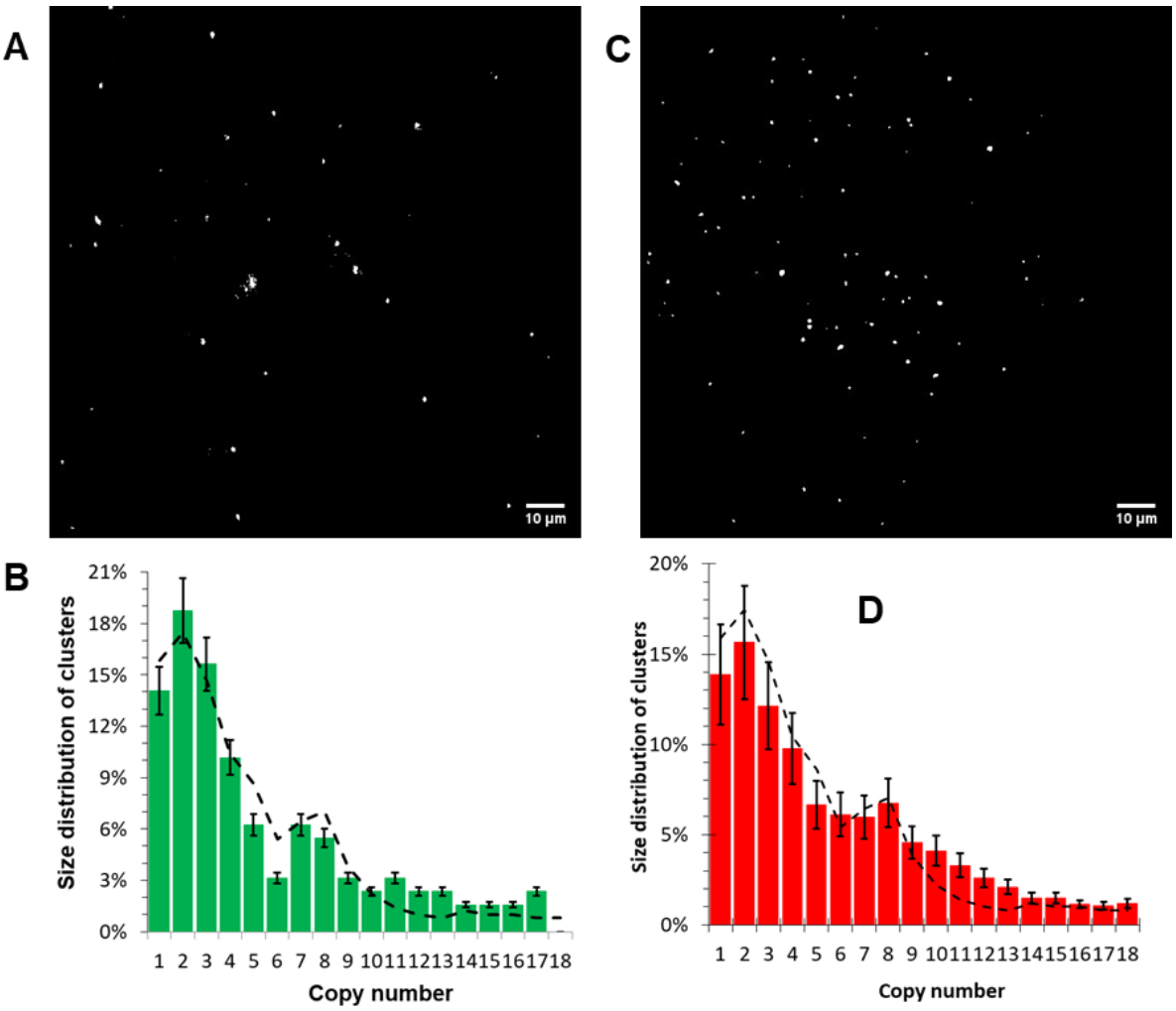
A
10 µm
C
10 µm
B
Size distribution of clusters
21%
18%
15%
12%
9%
6%
3%
0%
1 2 3 4 5 6 7 8 9 10 11 12 13 14 15 16 17 18
Copy number
D
Size distribution of clusters
20%
15%
10%
5%
0%
1 2 3 4 5 6 7 8 9 10 11 12 13 14 15 16 17 18
Copy number

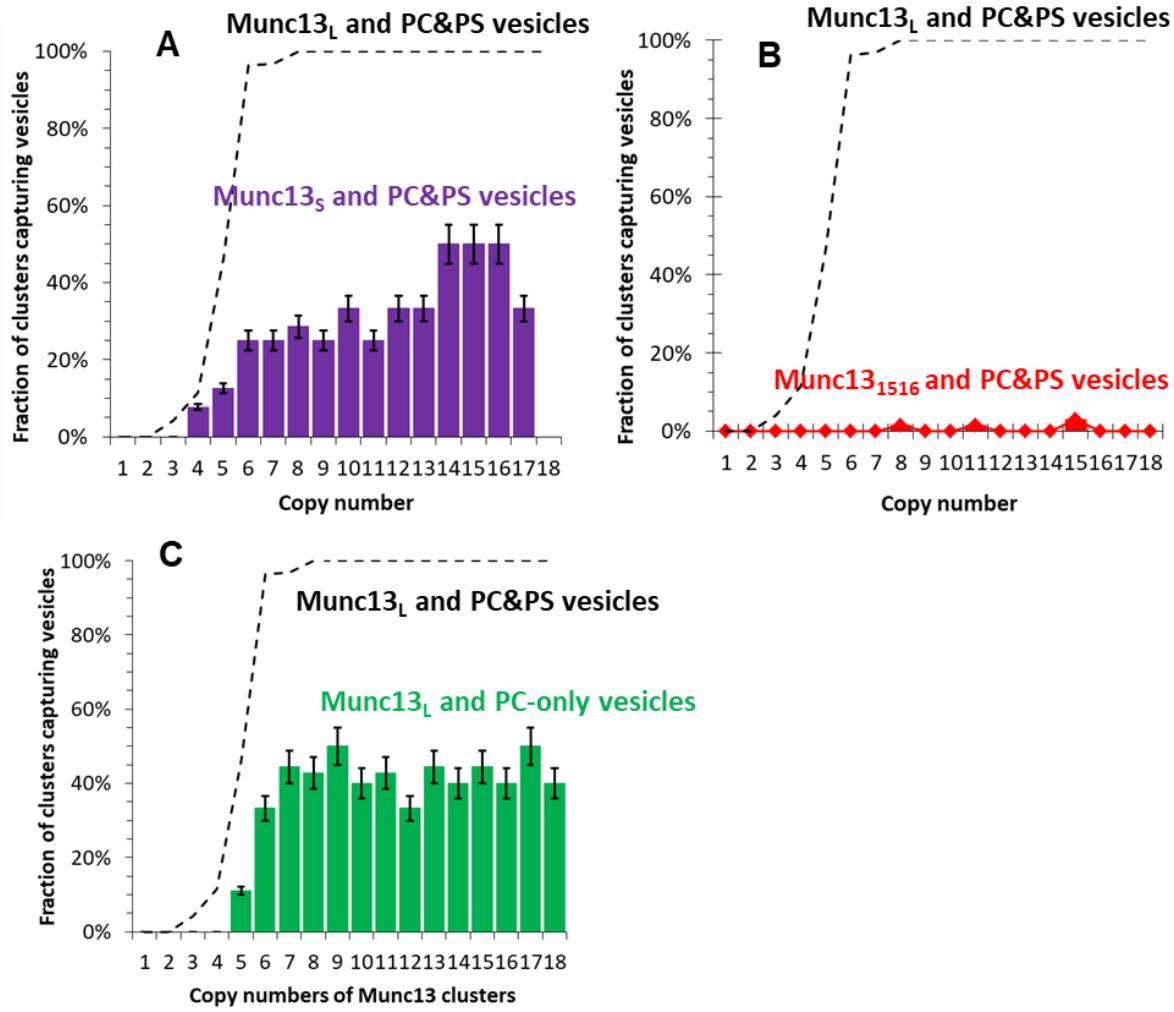
A
Munc13L and PC&PS vesicles
Munc13S and PC&PS vesicles
Fraction of clusters capturing vesicles
100%
80%
60%
40%
20%
0%
1 2 3 4 5 6 7 8 9 10 11 12 13 14 15 16 17 18
Copy number
B
Munc13L and PC&PS vesicles
Munc13 1516 and PC&PS vesicles
Fraction of clusters capturing vesicles
Copy number
C
Munc13L and PC&PS vesicles
Munc13L and PC-only vesicles
Fraction of clusters capturing vesicles
Copy numbers of Munc13 clusters

Supplementary Information for

Vesicle capture by membrane-bound Munc13-1 requires self-assembly into discrete clusters

Feng Li, Venkat Kalyana Sundaram, Alberto T. Gatta, Jeff Coleman, Sathish Ramakrishnan, Shyam S. Krishnakumar, Frederic Pincet, and James E. Rothman

Frederic Pincet and James E. Rothman
Email: frederic.pincet@yale.edu and james.rothman@yale.edu

This PDF file includes:

Figures S1 to S8
Legends for Movies S1 to S2

Other supplementary materials for this manuscript include the following:

Movies S1 to S2

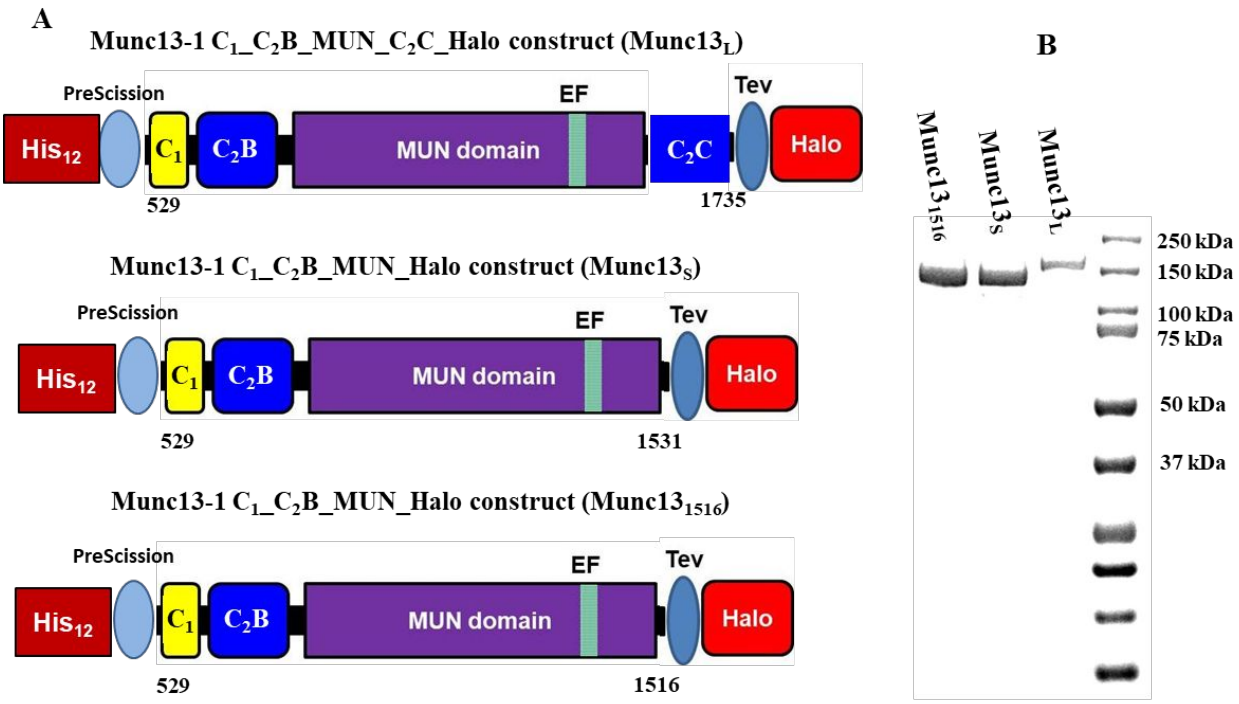

Fig. S1. (A) Munc13-1 constructs. **(B)** SDS-PAGE analysis of purified Munc13-1 proteins.

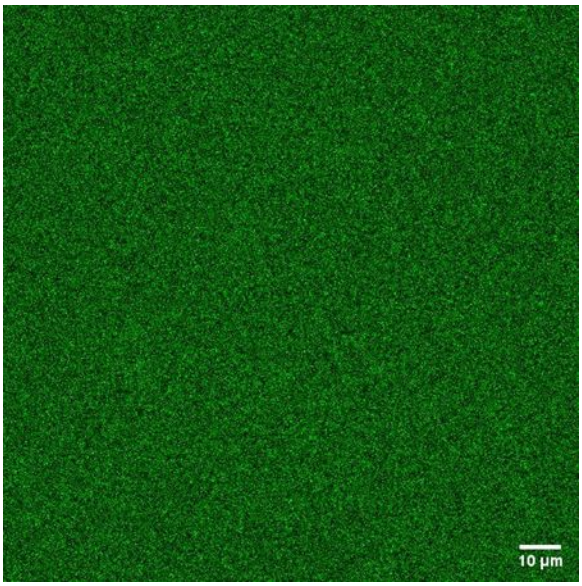

Fig. S2. A confocal image of supported bilayer containing DOPC, DOPS, DAG, PIP2 and DOPE-NBD.

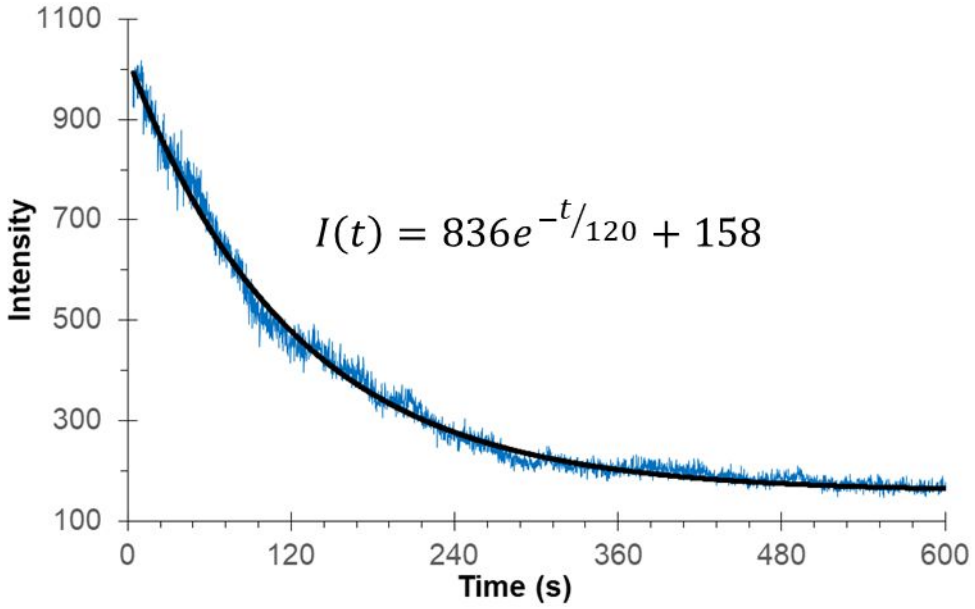

Fig. S3. Fitting of the fluorescent bleaching curve *I(t)* vs. *t* to find *I(0)*. The experimental bleaching data (blue curve) was fitted with an exponential equation $I = 836e^{-t/120} + 158$. Hence *I(0)* was 836.

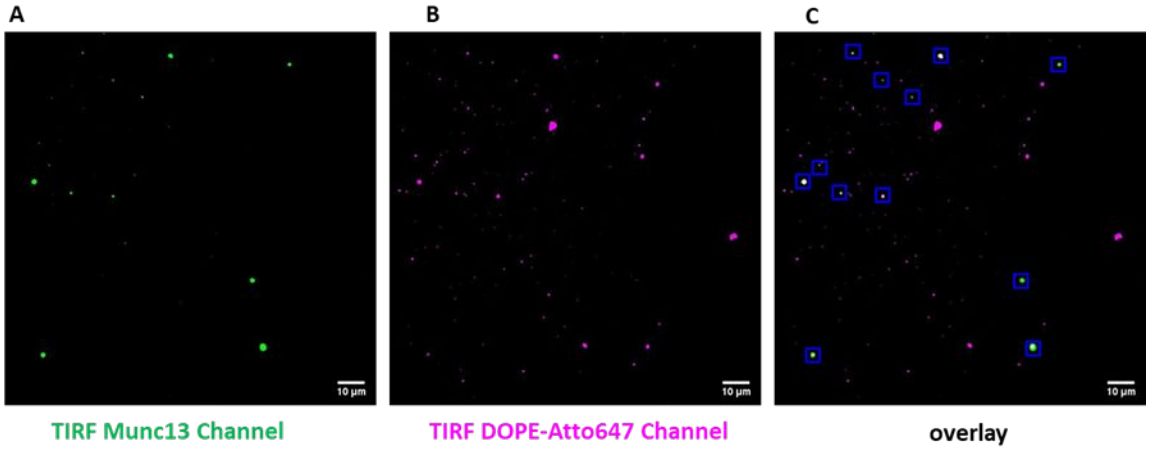

Fig. S4. VAMP2 and Synaptotagmin-1 do not affect Munc13-1's vesicle capturing. (A) TIRF image of clusters formed by $Munc13_L$ (residues 529 to 1735) labeled with Alexa 488 on lipid bilayer. **(B)** TIRF image of vesicles containing DOPC, DOPS, DOPE-Atto647N, VAMP2,and Synaptotagmin-1. Full length VAMP2 and Synaptotagmin-1 were reconstituted to vesicles via their transmembrane domains. **(C)** Merge of the previous two images. The blue boxes indicate the $Munc13_L$ clusters that co-localized with vesicles.

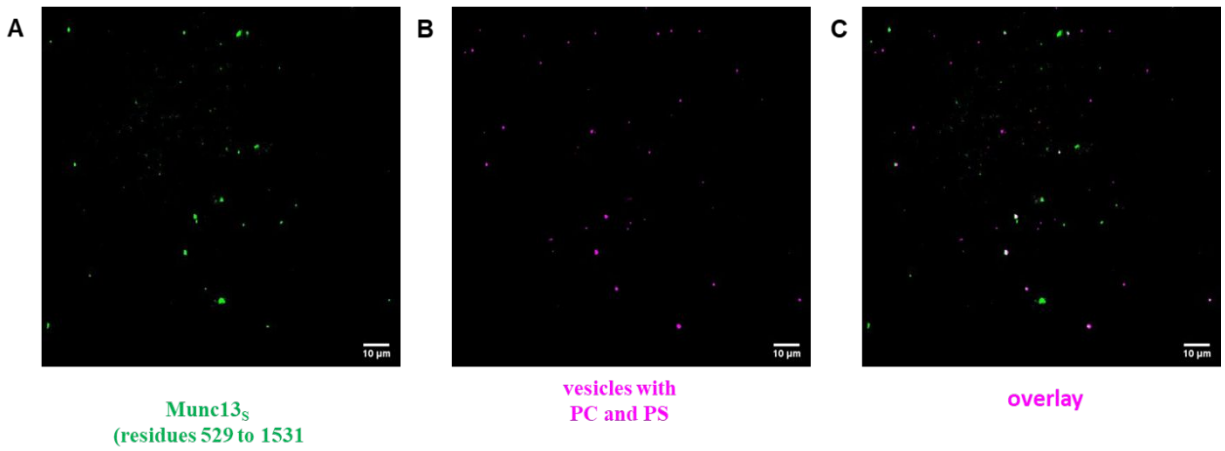

Fig. S5. C_2C domain affects Munc13-1's function of capturing vesicles. (A) TIRF image of clusters formed by $Munc13_S$ (residues 529 to 1531) labeled with Alexa488 on lipid bilayer. (B) TIRF image of vesicles containing PC and PS that are anchored to lipid bilayer. (C) Merge of the previous two images, which shows that $Munc13_S$ clusters capture fewer vesicles in the absence of C_2C domain.

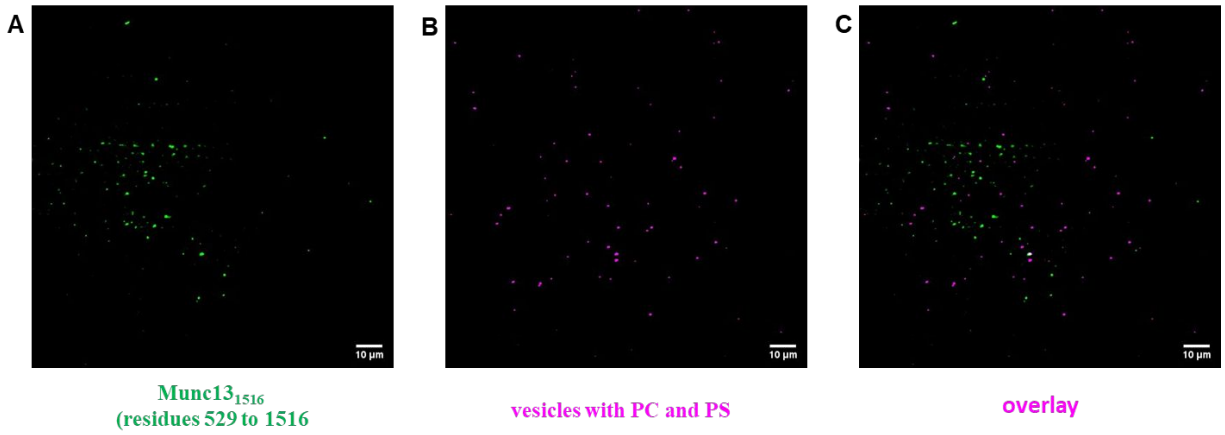

Fig. S6. Deletion of the hydrophobic end of MUN domain further reduces Munc13-1's function of capturing vesicles. (A) TIRF image of clusters formed by Munc13$_{1516}$ (residues 529 to 1516) labeled with Alexa488 on lipid bilayer. (B) TIRF image of vesicles containing PC and PS that are anchored to lipid bilayer. (C) Merge of the previous two images, which shows that Munc13$_{1516}$ clusters capture fewer vesicles in the absence of C_2C domain.

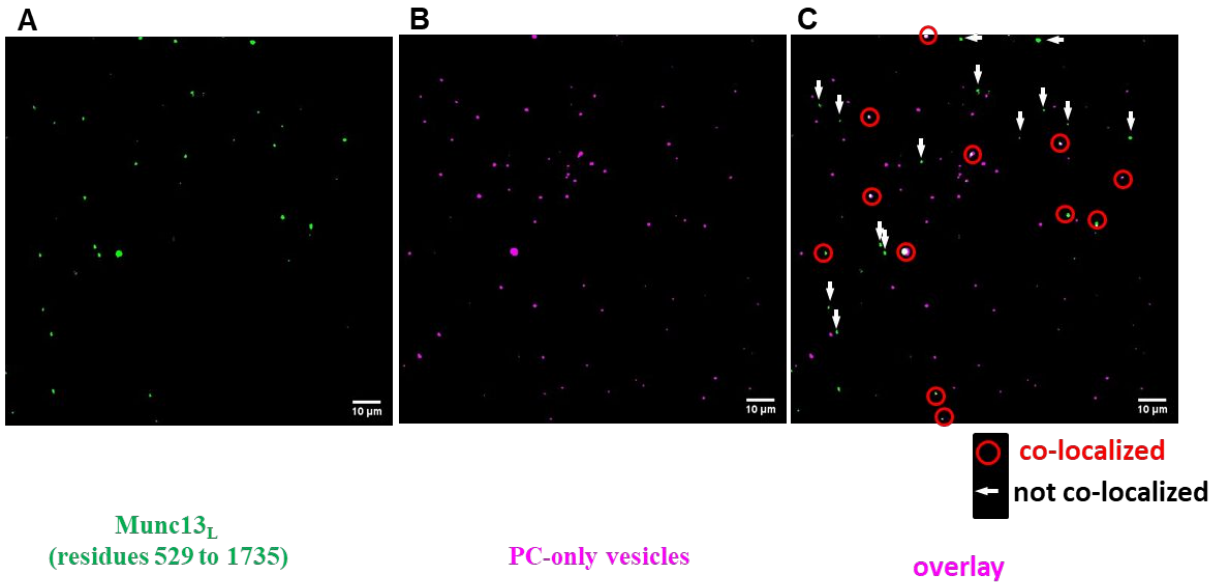

Fig. S7. Munc13$_L$ clusters still capture PC-only vesicles, but with reduced efficiency, . (A) TIRF image of clusters formed by Munc13$_L$ (residues 529 to 1735) labeled with on lipid bilayer. (B) TIRF image of PC-only vesicles that are anchored to lipid bilayer. (C) Merge of the previous two images, which shows that Munc13$_L$ clusters capture fewer vesicles as PS is removed from vesicles.

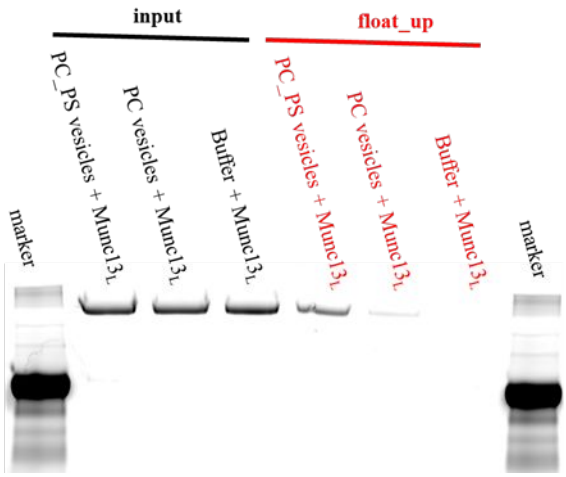

Fig. S8. **SDS-PAGE and fluorescence analysis of Munc13$_L$ floatation products.** Soluble Munc13$_L$ (labeled with Alexa488) were incubated with PC_PS vesicles (68% DOPC, 30% DOPS, 2% DOPE-Atto647N), PC vesicles (98% DOPC, 2% DOPE-Atto647N), and buffer, respectively, and then were centrifuged in nycodenz gradient. The input mixtures and float up products were loaded to a Bis-Tris, respectively, separated by electrophoresis, and imaged using 488 nm wavelength.

Movie S1 (separate file). Representative bleaching of $Munc13_L$ clusters formed on lipid bilayer (replay at 8x speed).

Movie S2 (separate file). Representative bleaching of clusters by $Munc13_S$ ΔC_2C formed on lipid bilayer (replay at 8x speed).